Chapter 2
Time-Interleaved ADCs

The time-interleaved ADC is an architecture that cycles through a set of N sub-ADCs, such that the aggregate throughput is N times the sample rate of the individual sub-ADCs [5]. Therefore, such an architecture enables the sample rate to be pushed further than that achievable with single channel ADCs. This chapter discusses the operation of time-interleaved ADCs and analyzes how the sub-ADCs interact. It also analyzes the drawbacks of the architecture and presents closed-form equations relating performance degradation to mismatch.

2.1 Modeling the Time-Interleaved ADC

This section discusses the operation of the time-interleaved ADC. The model presented serves as a foundation that allows the inclusion of time-varying errors due to differences between the sub-ADCs, as discussed in Sect. 2.2.

The time-interleaved ADC, as shown in Fig. 2.1a, has an input $x(t)$ and an output $y[n]$. The sampling period of the time-interleaved ADC and the N sub-ADCs are T_s and $\hat{T}_s = N \cdot T_s$, respectively. The ith sub-ADC, where $i = 0, ..., N-1$, is strobed with clock $\phi_i(t)$, which ideally has sampling edges at

$$\begin{aligned} t_i[n] &= n\hat{T}_s + iT_s \\ &= (nN + i) \cdot T_s \end{aligned} \tag{2.1}$$

Thus, the sampling edges of two consecutive clocks are offset by T_s, as in Fig. 2.1b, and the input signal is uniformly sampled. The output of the ith sub-ADC is $\hat{y}_i[n]$, where

$$\begin{aligned} \hat{y}_i[n] &= x\Big(t_i[n]\Big) \\ &= x\Big([nN + i] \cdot T_s\Big) \end{aligned} \tag{2.2}$$

M. El-Chammas and B. Murmann, *Background Calibration of Time-Interleaved Data Converters*, Analog Circuits and Signal Processing, DOI 10.1007/978-1-4614-1511-4_2,

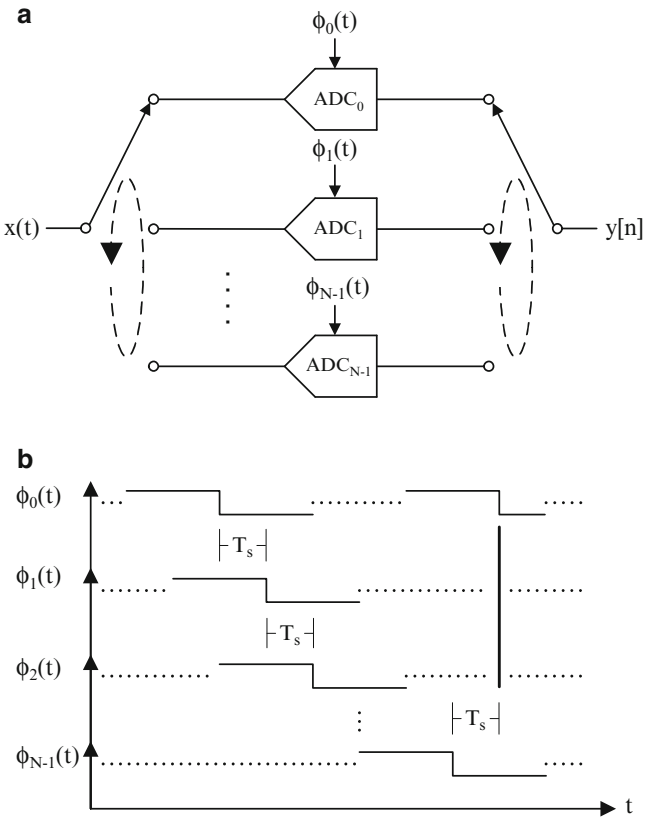

Fig. 2.1 (**a**) Time-interleaved ADC. (**b**) Sampling edges of sub-ADC clocks

The sub-ADC outputs $\hat{y}_i[n]$ are multiplexed to create $y[n]$, such that

$$y[n] = \hat{y}_i\left[\frac{n-i}{N}\right] \text{ where } i = n \bmod N \tag{2.3}$$

Setting $y_i[n]$ as the sub-ADC output $\hat{y}_i[n]$ upsampled by N results in

$$y_i[n] = \begin{cases} \hat{y}_i\left[\frac{n-i}{N}\right] & \text{if } \frac{n-i}{N} \text{ is an integer} \\ 0 & \text{else} \end{cases} \tag{2.4}$$

This is simplified by defining

$$\delta_i[n] = \sum_{k=-\infty}^{\infty} \delta[n - kN - i] \tag{2.5}$$

such that

$$y_i[n] = x(nT_s) \cdot \delta_i[n] \tag{2.6}$$

Thus, the time-interleaved ADC output $y[n]$ in (2.3) becomes

$$y[n] = \sum_{i=0}^{N-1} y_i[n] \tag{2.7}$$

As expected, the output of the ideal time-interleaved ADC reduces to $y[n] = x(nT_s)$.

2.1.1 Frequency Domain Analysis

The discrete-time Fourier transform (DTFT) is used to represent the time-interleaved ADC discrete-time output $y[n]$ and the sub-ADC output $y_i[n]$ in the frequency domain [6]. In general, the DTFT of a discrete-time input $x[n]$ [7] is

$$X(f) = \sum_{n=-\infty}^{\infty} x[n] \cdot e^{-j(2\pi f)n} \tag{2.8}$$

where $X(f)$ is periodic with period 1. The inverse transform is

$$x[n] = \int_{-1/2}^{1/2} X(f) \cdot e^{j(2\pi f)n} df \tag{2.9}$$

2.1.1.1 Sub-ADC Output

The DTFT of the upsampled sub-ADC output $y_i[n]$ in (2.6) is

$$Y_i(f) = \sum_{n=-\infty}^{\infty} (x[n]\delta_i[n]) \cdot e^{-j(2\pi f)n} \tag{2.10}$$

where $x[n] = x(nT_s)$. By property of the DTFT [7], $Y_i(f)$ is equal to the convolution of the DTFTs of $x[n]$ and $\delta_i[n]$. The DTFT of the sampled input $x[n]$ is $X(f)$, whereas the DTFT of $\delta_i[n]$ [8] is

$$D_i(f) = \frac{1}{N} \sum_{k=-\infty}^{\infty} \delta\left(f - \frac{k}{N}\right) \cdot e^{j\left(\frac{2\pi k}{N}\right)i} \tag{2.11}$$

such that

$$\begin{aligned} Y_i(f) &= X(f) * D_i(f) \\ &= \frac{1}{N} \sum_{k=-\infty}^{\infty} e^{j\left(\frac{2\pi k}{N}\right)i} \cdot X\left(f - \frac{k}{N}\right) \end{aligned} \tag{2.12}$$

This results in replicas at spacings of $\frac{2\pi k}{N}$ because of the subsampling behavior of the sub-ADCs. A phase-shift exists as a function of i, due to the exponential, such that, even though the magnitude of $Y_i(f)$ is the same for all the sub-ADCs, the phases are different.

2.1.1.2 Time-Interleaved ADC Output

The DTFT of the time-interleaved ADC output $y[n]$ in (2.7) is

$$Y(f) = \sum_{i=0}^{N-1} Y_i(f) \tag{2.13}$$

and, using (2.12), can be written as

$$Y(f) = \sum_{k=-\infty}^{\infty} M[k] \cdot X\left(f - \frac{k}{N}\right) \tag{2.14}$$

where $M[k]$ is defined as

$$\begin{aligned} M[k] &= \frac{1}{N} \sum_{i=0}^{N-1} e^{j\left(\frac{2\pi k}{N}\right)i} \\ &= \begin{cases} 1 & \text{if } \frac{k}{N} \text{ is an integer} \\ 0 & \text{else} \end{cases} \end{aligned} \tag{2.15}$$

Thus,

$$Y(f) = \sum_{k=-\infty}^{\infty} X\left(f - k\right) \tag{2.16}$$

and the inverse DTFT of $Y(f)$ is $x[n]$, as expected.

2.1.1.3 Interpretation

The sub-ADC outputs in (2.12) have frequency domain replicas with spacings of $\frac{2\pi k}{N}$. Due to the phase differences between the sub-ADC outputs, which are a function of i, all replicas except those at $2\pi k$ cancel when the sub-ADC outputs

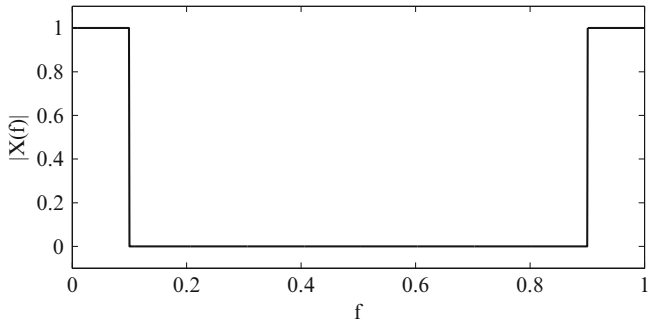

Fig. 2.2 Input signal DTFT example

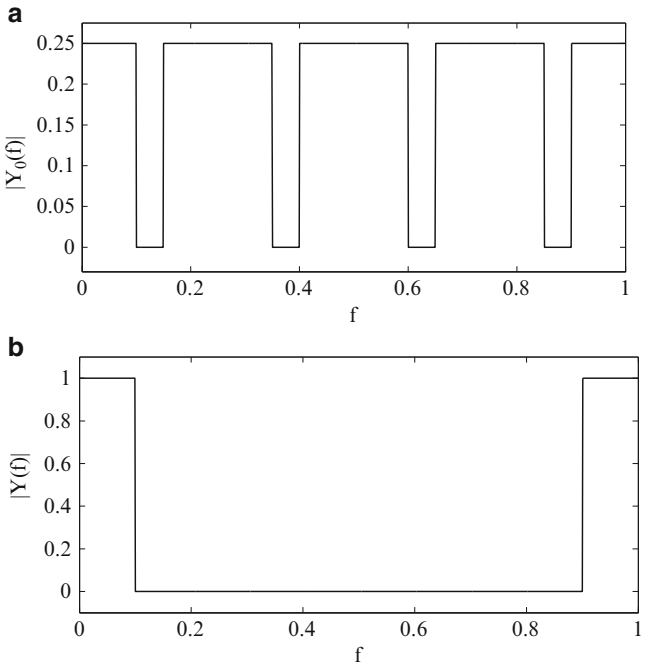

Fig. 2.3 Plotted DTFT of (**a**) a sub-ADC output and (**b**) the time-interleaved ADC output

are summed in (2.13). To illustrate this, assume that a 4-way time-interleaved ADC samples an input signal with a DTFT as in Fig. 2.2. As shown in Fig. 2.3a, the DTFT of the sub-ADC output consists of scaled replicas, whereas the resulting time-interleaved ADC output spectrum in Fig. 2.3b is identical to the input signal DTFT.

2.2 The Effect of Time-Varying Errors

As previously mentioned, and as in Fig. 2.1a, the inputs and outputs of the time-interleaved ADC are $x(t)$ and $y[n]$, respectively, where ideally $y[n] = x(nT_s)$, T_s being the sampling period of the time-interleaved ADC. Each of the N sub-ADCs is controlled by a clock with period $\hat{T}_s = N \cdot T_s$; the ideal phase offset of the clock for the ith sub-ADC with respect to the first sub-ADC is iT_s, where $i = 0, ..., N-1$. However, as illustrated in Fig. 2.4, there are several sources of mismatch in the signal data path which degrade the ADC performance. Each sub-ADC has its own gain G_i, offset o_i, and timing skew τ_i [5], which modify (2.6) into

$$y_i[n] = \Big(G_i \cdot x(nT_s - \tau_i) + o_i\Big) \cdot \delta_i[n] \tag{2.17}$$

for $i = 0, \ldots, N-1$. The effect of these errors can be viewed in the time domain, as in Fig. 2.5.

This section uses the frequency domain to develop a more intuitive understanding of how the outputs of the mismatched sub-ADCs interact and the time-domain to quantify the relationship between mismatch and ADC performance.

2.2.1 *Frequency Domain Analysis*

The ith sub-ADC output in (2.17) can be rewritten as

$$y_i[n] = \Big(h_i(nT_s) * x(nT_s) + o_i\Big) \cdot \delta_i \tag{2.18}$$

where o_i is the sub-ADC offset and $h_i(t)$ is a linear time-invariant function that is used to model both the sub-ADC gain and timing skew. It can also be used to

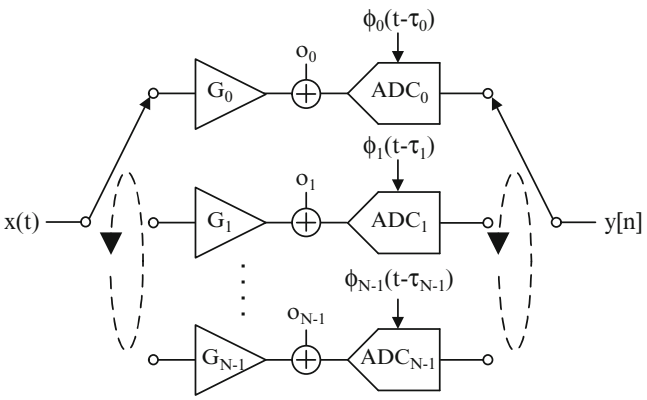

Fig. 2.4 Gain, offset, and timing skew in an N-channel time-interleaved ADC

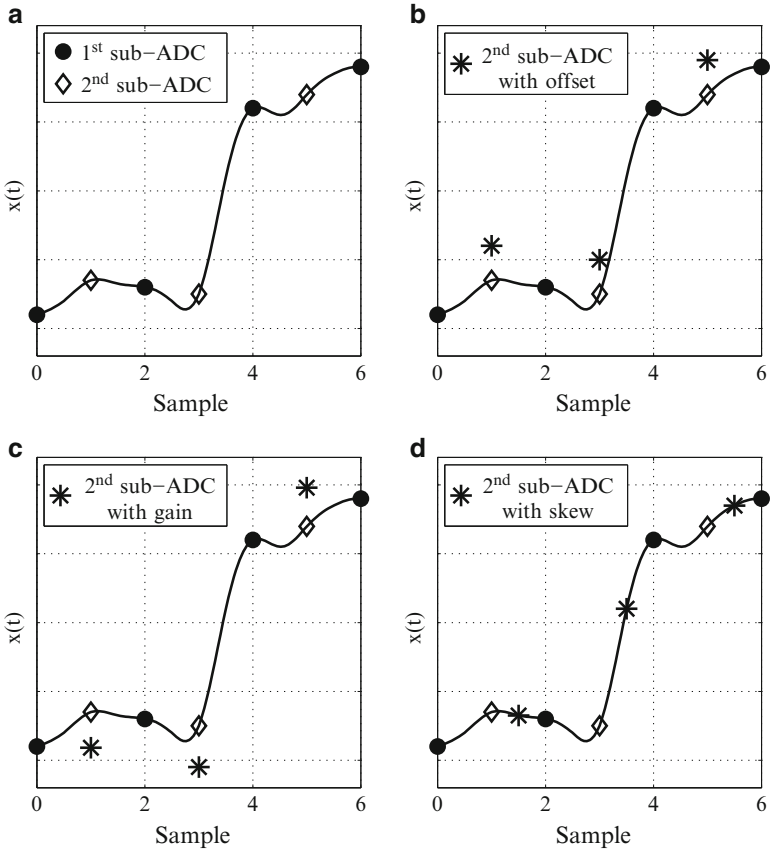

Fig. 2.5 Effect of mismatch on sampled signal with $N = 2$. (**a**) With no mismatch. (**b**) With offset mismatch. (**c**) With gain mismatch. (**d**) With timing skew

model other effects, such as bandwidth mismatch [9], although this is not discussed here. For example, gain is modeled with $h_i(t) = G_i \cdot \delta(t)$ and timing skew with $h_i(t) = \delta(t - \tau_i)$. When these effects are included, the DTFT of $y_i[n]$ in (2.12) becomes

$$Y_i(f) = \sum_{n=-\infty}^{\infty} \Big((h_i(nT_s) * x(nT_s) + o_i) \cdot \delta_i[n] \Big) \cdot e^{-j(2\pi f)n} \tag{2.19}$$

Defining $O_i(f)$ as

$$O_i(f) = o_i \cdot D_i(f) \tag{2.20}$$

where $D_i(f)$ is as in (2.11), and $\hat{X}_i(f)$ as the DTFT of $h_i(nT_s) * x(nT_s)$ such that

$$\hat{X}_i(f) = H_i(f) \cdot X(f) \tag{2.21}$$

simplifies $Y_i(f)$ into

$$Y_i(f) = \frac{1}{N} \sum_{k=-\infty}^{\infty} e^{j\left(\frac{2\pi k}{N}\right)i} \cdot \hat{X}_i\left(f - \frac{k}{N}\right) + O_i(f) \tag{2.22}$$

Therefore, the time-interleaved ADC output $y[n]$ has a DTFT of

$$\begin{aligned} Y(f) &= \sum_{i=0}^{N-1} Y_i(f) \\ &= \sum_{k=-\infty}^{\infty} M_h[k] \cdot X\left(f - \frac{k}{N}\right) + \sum_{i=0}^{N-1} O_i(f) \end{aligned} \tag{2.23}$$

where

$$M_h[k] = \frac{1}{N} \sum_{i=0}^{N-1} H_i\left(f - \frac{k}{N}\right) \cdot e^{j\left(\frac{2\pi k}{N}\right)i} \tag{2.24}$$

This is a generic setup for the errors in time-interleaved ADCs. As is seen in (2.24), the phases of the different sub-ADCs do not necessarily cancel out as they did in the ideal time-interleaved ADC because of $H_i(f)$, which is no longer unity. The three cases of offset, gain and timing skew will individually be expanded on.

2.2.1.1 Effect of Offset Mismatch

With offset mismatch, $h_i(t) = \delta(t)$ such that $H_i(f) = 1$, and $o_i \neq 0$. Therefore, $M_h[k]$ in (2.24) simplifies to (2.15), and

$$Y(f) = \sum_{k=-\infty}^{\infty} X(f - k) + \sum_{i=0}^{N-1} O_i(f) \tag{2.25}$$

The resulting spectrum has tones spaced at $\frac{2\pi k}{N}$, due to $O_i(f)$. These tones are not a function of the input signal, and only depend on the size of the offsets and the number of sub-ADCs. For example, using the input spectrum of Fig. 2.2, the resulting output with an interleaving factor of four and with offset mismatch is as shown in Fig. 2.6.

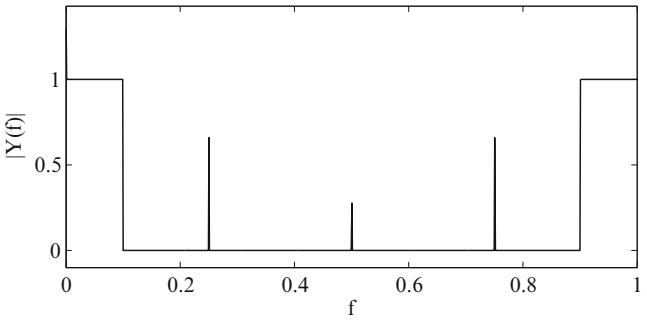

Fig. 2.6 Time-interleaved ADC output with offset mismatch

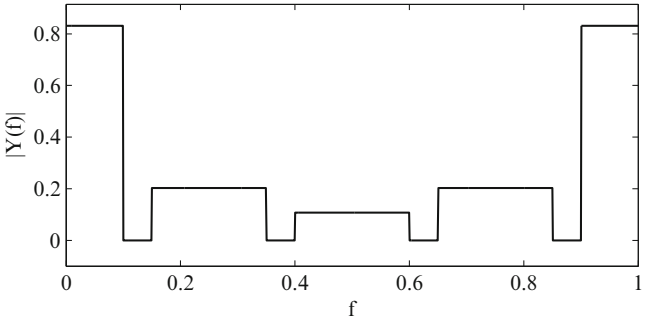

Fig. 2.7 Time-interleaved ADC output with gain mismatch

2.2.1.2 Effect of Gain Mismatch

With gain mismatch, $h_i(t) = G_i\delta(t)$ such that $H_i(f) = G_i$, and $o_i = 0$. Therefore,

$$Y(f) = \sum_{k=-\infty}^{\infty} M_h[k] \cdot X\left(f - \frac{k}{N}\right) \tag{2.26}$$

where

$$M_h[k] = \frac{1}{N}\sum_{i=0}^{N-1} G_i \cdot e^{j\left(\frac{2\pi k}{N}\right)i} \tag{2.27}$$

If $G_i = 1$ for all the sub-ADCs, then $M_h[k]$ becomes $M[k]$, as previously defined. However, when the gains are not all identical, the replicas in the sub-ADC outputs do not necessarily cancel out. The magnitude of these residual replicas is a function of the sub-ADC gains, such that the gain errors effectively amplitude modulate the input signal. For example, Fig. 2.7 plots the resulting output DTFT for an ADC with gain mismatch and an interleaving factor of four, using the input signal of Fig. 2.2. As is expected non-zero replicas exist because of gain errors.

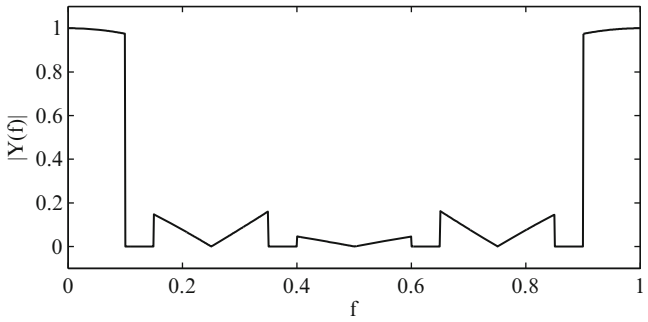

Fig. 2.8 Time-interleaved ADC output with timing skew

2.2.1.3 Effect of Timing Skew

With timing skew, $h_i(t) = \delta(t - \tau_i)$ such that $H_i(f) = e^{-j(2\pi f)\tau_i}$, and $o_i = 0$. Therefore,

$$Y(f) = \sum_{k=-\infty}^{\infty} M_h[k] \cdot X\left(f - \frac{k}{N}\right) \tag{2.28}$$

where

$$M_h[k] = \frac{1}{N} \sum_{i=0}^{N-1} e^{-j2\pi\left(f-\frac{k}{N}\right)\tau_i} \cdot e^{j\left(\frac{2\pi k}{N}\right)i} \tag{2.29}$$

If $\tau_i = 0$ for all the sub-ADCs, then $M_h[k]$ becomes $M[k]$, as previously defined. However, when the timing skews are not all identical, the replicas in the sub-ADC outputs do not cancel. The phases of these replicas are a function of the timing skews, effectively phase modulating the input signal. For example, Fig. 2.8 plots the resulting output DTFT for an ADC with timing skew and an interleaving factor of four, using the input signal of Fig. 2.2. In addition to having non-zero replicas, the baseband signal is slightly distorted, which is a result of the frequency dependent phase shifts caused by timing skew.

2.3 Quantitative Error Analysis

Analytic expressions quantifying the effect of the aforementioned time-varying errors on ADC performance are important when analyzing the design space of the time-interleaved ADC. This section relates the ADC *SNR* to these errors, and provides statistical bounds on the acceptable mismatch.

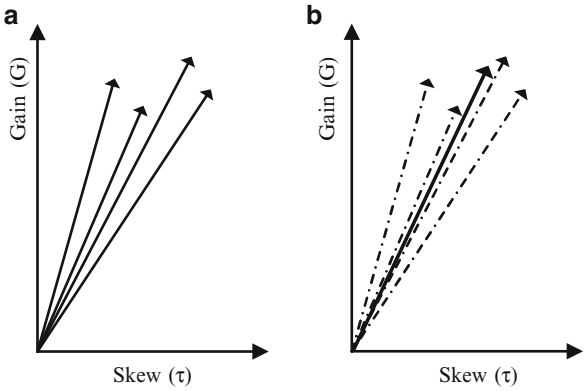

Fig. 2.9 (**a**) Vector representation for sub-ADC mismatch assuming $N = 4$. (**b**) "Best Fit" vector is the *solid arrow*, and is obtained by minimizing the mean-square error with all the sub-ADC vectors

2.3.1 *Error Analysis Method*

Analyzing the effect of time-varying errors consists of writing the output $y[n]$ of the time-interleaved ADC in terms of two components [10] as

$$y[n] = x_o[n] + e[n] \tag{2.30}$$

where $x_o[n]$ is a uniformly sampled version of the incoming signal $x(t)$ and is the "best fit" to the time-interleaved ADC output $y[n]$ such that

$$x_o[n] = \hat{G} \cdot x(nT - \hat{\tau}) \tag{2.31}$$

and where $e[n]$ is the resulting error signal. In other words, this "best fit" is a scaled and shifted version of the original input signal. For example, if the input $x(t)$ is a sinusoidal function, then the "best fit" $x_o[n]$ in (2.31) is also a sinusoidal function and suffers from no distortion harmonics. $\hat{G}$ and $\hat{\tau}$ are derived by maximizing the output *SNR*, which is equivalent to minimizing the mean-square error, and result in $x_o[n]$ and $e[n]$ being orthogonal [11]. This method is used for all relevant mismatches, and the results obtained subsume the approach in which only a sinusoid is used as an input.

Graphically, this can be viewed with a vector space representation. Each of the N sub-ADCs is represented by a two-dimensional vector (G_i, τ_i), as in Fig. 2.9a. The "best fit" is then the vector that minimizes the mean-square error, as in Fig. 2.9b. It is interesting to note that if $G_i = G$ and $\tau_i = \tau$, regardless of what G and τ actually are, then $\hat{G} = G$ and $\hat{\tau} = \tau$, as is depicted by the vectors in Fig. 2.9b.

The input signal in this analysis is assumed to be WSS with signal power P and autocorrelation $R(\tau)$. Without loss of generality, the mean of the input signal is set to zero and mean of the sub-ADC gains is set to one, such that

$$E[x(t)] = 0 \tag{2.32}$$

and

$$\frac{1}{N} \cdot \sum_{i=0}^{N-1} G_i = 1 \tag{2.33}$$

Therefore, the mean of the error signal is

$$\begin{aligned} E\big[e[n]\big] &= E\big[y[n] - x_o[n]\big] \\ &= \frac{1}{N} \sum_{i=0}^{N-1} o_i \end{aligned} \tag{2.34}$$

The mean-square error is defined as

$$f(\hat{G}, \hat{\tau}) = E\Big[e[n]^2\Big] - E\Big[e[n]\Big]^2 \tag{2.35}$$

such that

$$f(\hat{G}, \hat{\tau}) = \left(\hat{G}^2 P + \frac{P}{N} \sum_{i=0}^{N-1} G_i^2 - 2\frac{\hat{G}}{N} \sum_{i=0}^{N-1} G_i R(\tau_i - \hat{\tau}) + \frac{1}{N} \sum_{i=0}^{N-1} o_i^2 \right) - \frac{1}{N^2} \left(\sum_{i=0}^{N-1} o_i \right)^2 \tag{2.36}$$

The mean-square error in (2.36) is minimized with respect to both $\hat{G}$ and $\hat{\tau}$ by first setting the partial derivative of (2.36)

$$\frac{\partial f(\hat{G}, \hat{\tau})}{\partial \hat{G}} = 2\hat{G} P - \frac{2}{N} \sum_{i=0}^{N-1} G_i R(\tau_i - \tau) \tag{2.37}$$

to zero. Therefore,

$$\hat{G} = \frac{1}{NP} \sum_{i=0}^{N-1} G_i R(\tau_i - \hat{\tau}) \tag{2.38}$$

This is optimal because (2.36) is convex in $\hat{G}$. The optimal "best fit" gain is thus a function of the individual sub-ADC gains and the autocorrelation of the input function.

$\hat{\tau}$ is then found by replacing (2.38) in (2.36) such that

$$f(\hat{G}, \hat{\tau}) = \frac{P}{N} \sum_{i=0}^{N-1} G_i^2 - \frac{1}{N^2 P} \left(\sum_{i=0}^{N-1} G_i R(\tau_i - \hat{\tau}) \right)^2 + \frac{1}{N} \sum_{i=0}^{N-1} o_i^2 - \frac{1}{N^2} \left(\sum_{i=0}^{N-1} o_i \right)^2 \tag{2.39}$$

and (2.39) is minimized by finding the value of $\hat{\tau}$ that maximizes $\sum_i G_i R(\tau_i - \hat{\tau})$ such that

$$\hat{\tau} = \arg\max_{\tau} \sum_{i=0}^{N-1} G_i R(\tau_i - \tau) \tag{2.40}$$

For input signals with a first-order differentiable autocorrelation function, this is equivalent to the value of $\hat{\tau}$ that satisfies

$$\sum_{i=0}^{N-1} G_i \frac{dR(\tau_i - \tau)}{d\tau}\bigg|_{\tau=\hat{\tau}} = 0 \tag{2.41}$$

Solutions obtained with (2.41) must be checked to see if they satisfy concavity constraints for maximization.

Using the values obtained for $\hat{G}$ and $\hat{\tau}$, we can directly solve for $SNR_f = P_S/P_N$, where $P_S = P$ and where $P_N = f(\hat{G}, \hat{\tau})$. In the context of ADCs, it is meaningful to quantify the effect of mismatches by comparing the resulting *SNR* to that due to quantization. In an ADC with a resolution of B bits, the *SNR* due to quantization is

$$SNR_Q = \frac{3}{2} \cdot \left(2^{2B}\right) \tag{2.42}$$

This is used to provide a bound on all three of the aforementioned mismatches by setting

$$SNR_f \geq SNR_Q \tag{2.43}$$

When equality exists in (2.43), the actual *SNR* (which includes the effect of quantization) is $SNR = SNR_f - 3\text{dB}$. The time-interleaved ADC is "quantization-noise limited" when strict inequality exists and is "mismatch limited" when $SNR_f < SNR_Q$. This presents a deterministic bound on the relevant mismatch, and can be used to validate a given converter. In other words, given a time-interleaved ADC with a set of gain, offset, or timing skew mismatch, and given the input signal autocorrelation function it is possible to state whether the converter is quantization-noise limited or mismatch limited.

However, it is also useful to know beforehand what the acceptable mismatch is for a time-interleaved ADC with a target resolution of B bits. This can be done by bounding the variance of the time-varying error with

$$E\left[f(\hat{G}, \hat{\tau})\right] \leq \left(\frac{2}{3}\right) \cdot \left(\frac{P}{2^{2B}}\right) \tag{2.44}$$

and by assuming that these errors are independent and identically distributed random variables. This is done for each of the time-varying errors in the sections below.

2.3.2 Impact of Offset

With the assumptions that the gain and timing skew for all N sub-ADCs are identical such that, without loss of generality, $G_i = 1$ and $\tau_i = 0$, the mean-square error in (2.39) reduces to

$$f(\hat{G}, \hat{\tau}) = \frac{1}{N} \sum_{i=0}^{N-1} o_i^2 - \frac{1}{N^2} \left(\sum_{i=0}^{N-1} o_i \right)^2 \tag{2.45}$$

Therefore, the *SNR* due to offset is

$$SNR_O = \frac{P}{\frac{1}{N} \sum_{i=0}^{N-1} o_i^2 - \frac{1}{N^2} \left(\sum_{i=0}^{N-1} o_i \right)^2} \tag{2.46}$$

and the statistical bound on the variance of offset, using (2.44), is

$$\sigma_o^2 \leq \left(\frac{N}{N-1} \right) \cdot \left(\frac{2 \cdot P}{3 \cdot 2^{2B}} \right) \tag{2.47}$$

Thus, the bound on offset is a function of the number of sub-ADCs N, the input signal power P, and the ADC resolution B. The bound on offset is unique when compared to that of both gain mismatch and timing skew since it is directly proportional to P. It is intuitive that ADCs with higher power input signals can cope with larger sub-ADC offsets. Furthermore, as shown in (2.47), higher resolution ADCs result in smaller bounds on offset mismatch, as does a higher interleaving factor, although the ADC resolution has a much larger effect on the bound. For example, if $P = 0.5\ V^2$, $B = 10$, and $N = 2$, then $\sigma_o \leq 0.8\,\text{mV}$.

2.3.3 Impact of Gain

With the assumptions that the offset and timing skew for all N sub-ADCs are identical such that, without loss of generality, $o_i = 0$ and $\tau_i = 0$, the mean-square error in (2.39) reduces to

$$f(\hat{G}, \hat{\tau}) = \frac{P}{N} \sum_{i=0}^{N-1} G_i^2 - \frac{P}{N^2} \left(\sum_{i=0}^{N-1} G_i \right)^2 \tag{2.48}$$

Therefore, the *SNR* due to gain is

$$SNR_G = \frac{1}{\frac{1}{N} \sum_{i=0}^{N-1} G_i^2 - \frac{1}{N^2} \left(\sum_{i=0}^{N-1} G_i \right)^2} \tag{2.49}$$

Note that the *SNR* due to gain mismatch is independent of the signal power, and only depends on the magnitude of the individual gains. The statistical bound on the variance of gain, using (2.44), is

$$\sigma_G^2 \leq \left(\frac{N}{N-1}\right) \cdot \left(\frac{2}{3 \cdot 2^{2B}}\right) \tag{2.50}$$

This is almost identical to (2.47) in that it is inversely proportional to both the ADC resolution B and the interleaving factor N. However, it does not depend on the signal power P or on any other signal information. For example, if $N = 2$ and $B = 10$, then $\sigma_G \leq 1.1\%$.

2.3.4 Impact of Timing Skew

The results from analyzing timing skew are more interesting than those of both gain and offset, as they depend on the "speed" of the input signal. With the gain and offset of all N sub-ADCs set to $G_i = 1$ and offset $o_i = 0$, the mean-square error is

$$f(\hat{G}, \hat{\tau}) = P - \frac{1}{N^2 P}\left(\sum_{i=0}^{N-1} R(\tau_i - \hat{\tau})\right)^2 \tag{2.51}$$

where

$$\hat{\tau} = \arg\max_{\tau} \sum_{i=0}^{N-1} R(\tau_i - \tau) \tag{2.52}$$

and thus the *SNR* is

$$SNR_\tau = \frac{1}{1 - \frac{1}{N^2}\left(\sum_{i=0}^{N-1} \frac{R(\tau_i - \hat{\tau})}{P}\right)^2} \tag{2.53}$$

The relationship between SNR_τ and the autocorrelation $R(\tau)$ in (2.53) is intuitive because the autocorrelation function reflects the "speed" of the signal. This is important since the speed, or the rate of change, of the input signal is directly proportional to the sampling error a given skew will create. For example, Fig. 2.10a shows a signal that does not change much for a certain value of τ, which leads to a small sampling error. This is captured by the autocorrelation $R(\tau)$, as in Fig. 2.10b, since $R(\tau)$ is close to 1. The signal in Fig. 2.10c changes significantly for a skew of τ. This is also captured by the autocorrelation $R(\tau)$, which, as in Fig. 2.10d, is not as close to 1.

A deterministic bound on timing skew is derived with

$$\frac{1}{P} \cdot \sum_{i=0}^{N-1} R(\tau_i - \hat{\tau}) \geq N\sqrt{\frac{SNR_Q - 1}{SNR_Q}} \tag{2.54}$$

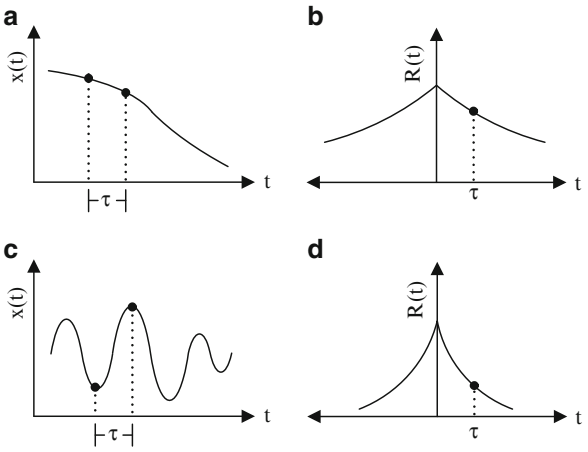

Fig. 2.10 (**a**) Slow signal. (**b**) Wide autocorrelation for slow signal. (**c**) Fast signal. (**d**) Narrow autocorrelation for fast signal

To calculate a statistical bound, it is useful to assume the autocorrelation is second-order differentiable, such that it can be expressed as a Taylor series centered around $\tau = 0$. Thus, when τ is small, we have

$$R(\tau) \approx R(0) + R'(0)\tau + \frac{R''(0)}{2}\tau^2 \tag{2.55}$$

where $R(0) = P$. Without loss of generality, $P = 1$. Since $R(\tau)$ is an even function and has a maximum at $\tau = 0$, $R'(0) = 0$ and $R''(0) \leq 0$. Therefore,

$$\frac{dR(\tau)}{d\tau} \approx R''(0)\tau \tag{2.56}$$

where $R''(0)$ is the curvature of the autocorrelation function.

Combining this with (2.41) allows us to solve for $\hat{\tau}$, such that

$$\sum_{i=0}^{N-1} R''(0)(\tau_i - \hat{\tau}) \approx 0$$

$$\hat{\tau} \approx \frac{1}{N}\sum_{i=0}^{N-1} \tau_i \tag{2.57}$$

Using (2.54) with (2.55) results in

$$\sum_{i=0}^{N-1}\left(1 + \frac{R''(0)}{2}(\tau_i - \hat{\tau})^2\right) \geq N\sqrt{\frac{SNR_Q - 1}{SNR_Q}} \tag{2.58}$$

and $R''(0)(\tau_i - \hat{\tau})^2$ can be expanded using (2.57) as

$$\begin{aligned} R''(0)(\tau_i - \hat{\tau})^2 &= R''(0)(\tau_i^2 + \hat{\tau}^2 - 2\tau_i\hat{\tau}) \\ &= R''(0)\left(\tau_i^2 + \frac{1}{N^2}\left(\sum_{i=0}^{N-1}\tau_i\right)^2 - 2\frac{\tau_i}{N}\left(\sum_{i=0}^{N-1}\tau_i\right)\right) \end{aligned} \tag{2.59}$$

Assuming the skews τ_i are independent and identically distributed random variables, with mean zero and variance σ_τ^2, the expected value of (2.58) is

$$E\left[\sum_{i=0}^{N-1} R(\tau_i - \hat{\tau})\right] \approx N + \frac{1}{2}R''(0)(N-1)\sigma_\tau^2 \tag{2.60}$$

and thus

$$N + \frac{1}{2}R''(0)(N-1)\sigma_\tau^2 \geq N\sqrt{\frac{SNR_Q - 1}{SNR_Q}} \tag{2.61}$$

Since

$$\sqrt{\frac{SNR_Q - 1}{SNR_Q}} \approx \left(1 - \frac{1}{2SNR_Q}\right) \tag{2.62}$$

for large SNR_Q, the variance σ_τ^2 is bounded by

$$\sigma_\tau^2 \leq \left(\frac{N}{N-1}\right)\cdot\left(\frac{2}{3\cdot 2^{2B}}\right)\cdot\left(\frac{1}{|R''(0)|}\right) \tag{2.63}$$

This presents a closed-form bound on the acceptable variance of timing skew as a function of the number of sub-ADCs, the ADC resolution, and the curvature of the autocorrelation function, which is a property of the input signal statistics. Slower signals have smaller curvatures $R''(0)$, and thus have larger bounds.

Note that for a sinusoidal input with frequency f Hz, $R''(0) = -(2\pi f)^2$, and the bound on the variance $\hat{\sigma}_\tau^2$ using (2.63) is

$$\hat{\sigma}_\tau^2 \leq \left(\frac{N}{N-1}\right)\left(\frac{2}{3\cdot 2^{2B}(2\pi f)^2}\right) \tag{2.64}$$

which matches that obtained in [12].

2.3.4.1 Wide-Sense Cyclostationary Signals

The above results for timing skew were obtained for WSS signals, but it is also possible to extend them to wide-sense cyclostationary (WSCS) signals. This is a more realistic model for some communication signals, such as those present in serial

link receivers. A signal is WSCS if both its mean $m(t)$ and autocorrelation $R(t_1, t_2)$ are periodic in T [11], such that

$$m(t + T) = m(t) \tag{2.65}$$

$$R(t_1 + T, t_2 + T) = R(t_1, t_2) \tag{2.66}$$

For example, assume the autocorrelation of a zero-mean WSCS signal is periodic with the time-interleaved ADC sampling period T_s such that $R(t_1 + T_s, t_2 + T_s) = R(t_1, t_2)$. The ideal sampling phase of the first sub-ADC, which has previously been ignored because the input was WSS, is denoted by T_0, where $0 \leq T_0 < T_s$, such that the autocorrelation changes depends on what T_0 is. Minimizing the mean-square error as done in previous sections and as elaborated on in Appendix A, respectively modifies (2.38) and (2.52) into

$$\hat{G} = \frac{\sum_i R(T_0 - \hat{\tau}, T_0 - \tau_i)}{NR(T_0 - \hat{\tau}, T_0 - \hat{\tau})} \tag{2.67}$$

and

$$\hat{\tau} = \arg\max_{\tau} \frac{\left(\sum_{i=0}^{N-1} R(T_0 - \hat{\tau}, T_0 - \tau_i)\right)^2}{NR(T_0 - \hat{\tau}, T_0 - \hat{\tau})} \tag{2.68}$$

The *SNR* in (2.53) and the variance in (2.63) then become a function of T_0.

2.3.4.2 Jitter

It is also possible to use (2.63) in bounding the tolerable random clock jitter for a single ADC or time-interleaved array by taking the limit of $N \to \infty$. This follows by noting that jitter causes the ADC to sample the signal with a different random phase τ_i for its ith sample, which is equivalent to having a time-interleaved ADC with an infinite number of sub-ADCs, such that each sub-ADC has timing skew τ_i and samples the input signal once. Thus, the bound on jitter is

$$\sigma^2 \leq \left(\frac{2}{3 \cdot 2^{2B} |R''(0)|}\right) \tag{2.69}$$

This matches the result obtained by the authors of [13], who also show that using a sine wave in providing bounds on jitter overconstrains the variance bound by a factor of three when the input signal has a brick wall spectral density, as in (2.75). Equation (2.69) reduces to the known case of an input sine wave where $R''(0) = -(2\pi f)^2$ such that

$$\sigma^2 \leq \left(\frac{2}{3 \cdot 2^{2B} (2\pi f)^2}\right) \tag{2.70}$$

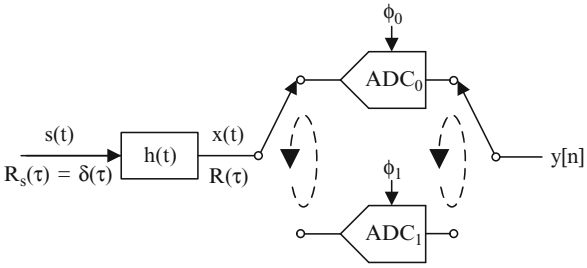

Fig. 2.11 Setup for simulation examples

2.3.5 Simulation Examples

This section illustrates the preceding analysis on the effect of timing skew with examples of WSS wideband input signals, which are applied to both the deterministic and the statistical bounds. These signals are formed by coloring white noise with linear time-invariant filters, as in Fig. 2.11. The time-interleaved ADC used in these examples has $N = 2$ sub-ADCs. An example with a WSCS signal is also shown.

2.3.5.1 Examples for Deterministic Bounds

Both an ideal filter and a first-order low pass filter are used in this section, which allows us to compare the *SNR* obtained with (2.53) to that obtained with Monte Carlo simulations.

2.3.5.2 Ideal Filter

In this example, white noise is passed through an ideal low pass filter with cutoff frequency f_c Hz; the resulting signal has an autocorrelation function of

$$R(\tau) = \text{sinc}(2f_c\tau) \tag{2.71}$$

Without loss of generality, we set $\tau_0 = 0$, which is the timing skew of the first sub-ADC. This allows us to vary the timing skew τ_1 of the second sub-ADC and plot the theoretical value of (2.53) as a function of τ_1 for different values of f_c. This theoretical *SNR* is compared to that obtained with Monte Carlo simulations in Fig. 2.12 for different values of f_c. As is expected, the *SNR* increases for a given τ_1 as f_c decreases.

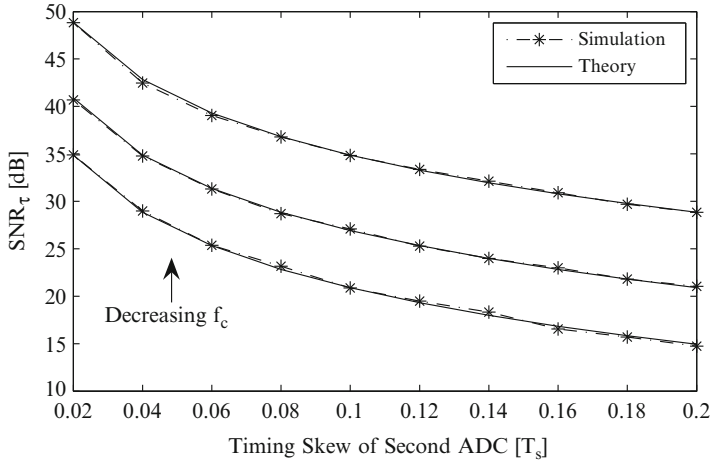

Fig. 2.12 Comparison of theoretical and simulation based SNR_τ with an input signal autocorrelation function of $R(\tau) = \text{sinc}(2f_c\tau)$, for $f_c = 0.1f_s, 0.25f_s$, and $0.5f_s$

2.3.5.3 First-Order Low Pass Filter

In this example, white noise is passed through a first-order low pass filter with a 3 dB frequency of $f_{3\text{dB}}$ Hz. The autocorrelation of such an input signal is

$$R(\tau) = e^{-(2\pi f_{3\text{dB}})|\tau|} \tag{2.72}$$

The theoretical *SNR* obtained by replacing this in (2.53) is compared to the *SNR* obtained through Monte Carlo simulations in Fig. 2.13 for different values of $f_{3\text{dB}}$. Again, the achievable *SNR* depends on both the timing skew and $f_{3\text{dB}}$.

2.3.5.4 Examples for Statistical Bounds

This section demonstrates the applicability of (2.63) for WSS signals that have a second-order differentiable autocorrelation function. The examples used are the ideal filter and the second-order low pass filter.

2.3.5.5 Ideal Filter

Because $R(\tau)$ in this example [as in (2.71)] is second-order differentiable, we have

$$R''(0) = -\frac{1}{3}(2\pi f_c)^2 \tag{2.73}$$

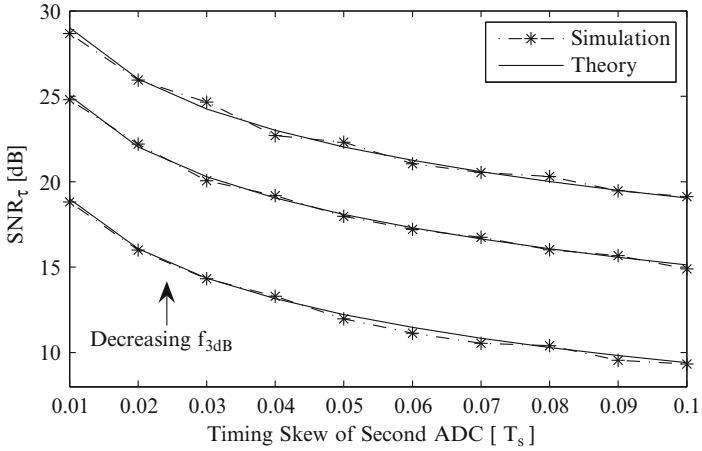

Fig. 2.13 Comparison of theoretical and simulation based SNR_τ with an input signal autocorrelation function of $R(\tau) = e^{-2\pi f_{3\text{dB}}|\tau|}$, for $f_{3\text{dB}} = 0.02f_s$, $0.05f_s$, and $0.2f_s$

Replacing this in (2.63) results in a statistical bound of

$$\sigma_\tau^2 \leq \left(\frac{N}{N-1}\right) \cdot \left(\frac{2}{2^{2B} \cdot (2\pi f_c)^2}\right) \tag{2.74}$$

Figure 2.14 shows how the ADC *SNR* is bounded by the sigma of the skew for different values of f_c as a function of f_s, the sampling frequency. It is worth looking at how the variance σ_τ^2 in (2.74) compares to that obtained with standard sinusoidal analysis. Since the input signal is bandlimited to f_c, standard analysis would use a sine wave of frequency f_c. The ratio of (2.74) to (2.64) is

$$\left(\frac{\sigma_\tau}{\hat{\sigma}_\tau}\right)^2 = 3 \tag{2.75}$$

Thus, using standard sinusoidal analysis in this example leads to over-constraining the acceptable bound on timing skew variance by a factor of three, which also matches the result obtained in [13].

2.3.5.6 Second-Order Low Pass Filter

The impulse response for a second-order low pass filter is

$$h(t) = te^{-(\omega_{3\text{dB}}t)}u(t) \tag{2.76}$$

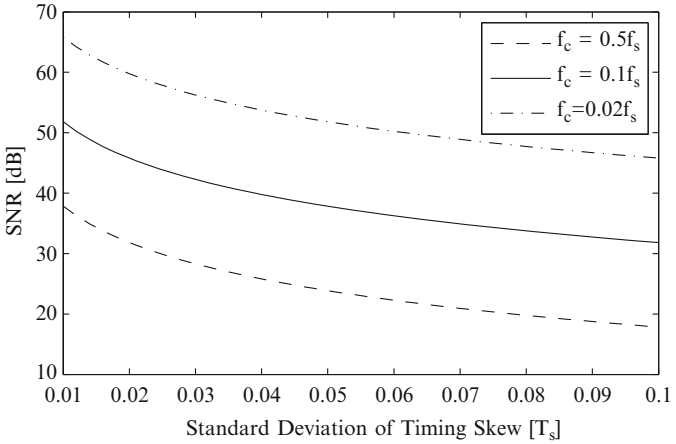

Fig. 2.14 ADC *SNR* as a function of the standard deviation of timing skew, which is calculated using equality in (2.74). Input signal is bandlimited white noise and has an autocorrelation function of $R(\tau) = \text{sinc}(2f_c\tau)$

where $\omega_{3\text{dB}} = 2\pi f_{3\text{dB}}$. The autocorrelation function for a second-order low pass filter, normalized such that R(0) = 1, is derived to be

$$R(\tau) = e^{-(|\tau|\omega_{3\text{dB}})} \cdot (1 + |\tau|\omega_{3\text{dB}}) \tag{2.77}$$

This is second-order differentiable, which allows us to calculate $R''(0)$ as

$$R''(0) = -(2\pi f_{3dB})^2 \tag{2.78}$$

Replacing this in (2.63) results in a statistical bound of

$$\sigma_\tau^2 \leq \left(\frac{N}{N-1}\right) \cdot \left(\frac{2}{3 \cdot 2^{2B} \cdot (2\pi f_{3\text{dB}})^2}\right) \tag{2.79}$$

A comparison to a sine wave is not as simple in this example as it is in the previous one, because the spectrum is nonzero for all frequencies. Therefore, assume that in the standard analysis, a sine wave with frequency $\hat{f}$ is used to calculate the bound on timing skew. This enables us to compare the bound on timing skew using (2.79) to that provided using (2.64) by setting $f_{3\text{dB}} = \alpha\hat{f}$. An interesting observation is that when $\alpha = 1$, or $f_{3\text{dB}} = \hat{f}$, the bound on skew is the same for both the second-order low pass filter and the sine wave input signal, even though the spectrum for the second-order low pass filter is still non-zero for frequencies larger than $\hat{f}$.

A more complete comparison is possible by looking at the ratio $\beta = \sigma_\tau/\hat{\sigma}_\tau$ as a function of α, as in Fig. 2.15, where σ_τ is defined in (2.79) and $\hat{\sigma}_\tau$ is defined in (2.64), such that

$$\beta = \frac{\sigma_\tau}{\hat{\sigma}_\tau} = \frac{1}{\alpha} \tag{2.80}$$

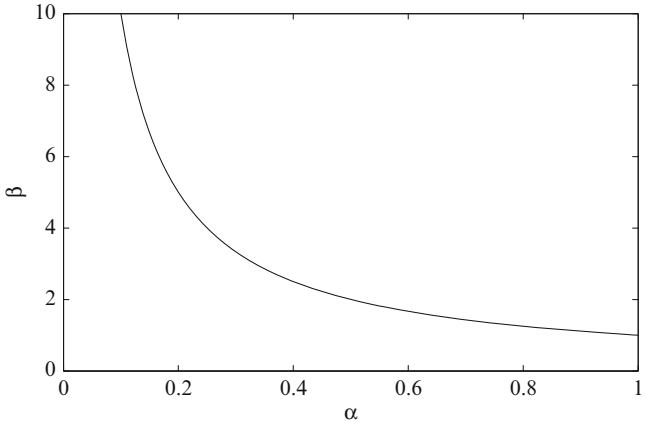

Fig. 2.15 Comparison of standard deviation of skew for second-order low pass filter and sine wave, where α is such that $f_{3\text{dB}} = \alpha \hat{f}$ and $\beta = \sigma_\tau / \hat{\sigma}_\tau$

For example, when $f_{3\text{dB}} = 0.5\hat{f}$, $\beta = 2$, which implies that standard analysis results in over-constraining the acceptable bound on the timing skew standard deviation by a factor of 2. In a more extreme example, when $f_{3\text{dB}} = 0.1\hat{f}$, $\beta = 10$.

This again demonstrates the importance of knowing the input signal statistics when deriving bounds on the acceptable timing skew. It is worth noting that even when $f_{3\text{dB}}$ is not exactly known, as may be the case with certain signals, the range in which $f_{3\text{dB}}$ falls can still be used. For example, if $0.1\hat{f} < f_{3\text{dB}} < 0.2\hat{f}$, then $10 > \beta > 5$.

2.3.5.7 Example of Deterministic Bound for WSCS Signals

In this example, an infinite series of bits $c_n \in \{-1, +1\}$, where $R_c(n, m) = E[c_n c_m] = \delta_{n-m}$ and $m_c = E[c_n] = 0$, are sent such that the transmitted signal is

$$s(t) = \sum_{m=-\infty}^{\lfloor t/T \rfloor} c_m p(t - mT) \tag{2.81}$$

where $p(t)$ is a rectangular pulse with length T and is defined by

$$p(t) = u(t) - u(t - T) \tag{2.82}$$

The transmitted signal s(t) passes through a linear time-invariant channel $h(t)$, as in Fig. 2.11, before the time-interleaved ADC can sample the signal $x(t)$. Thus,

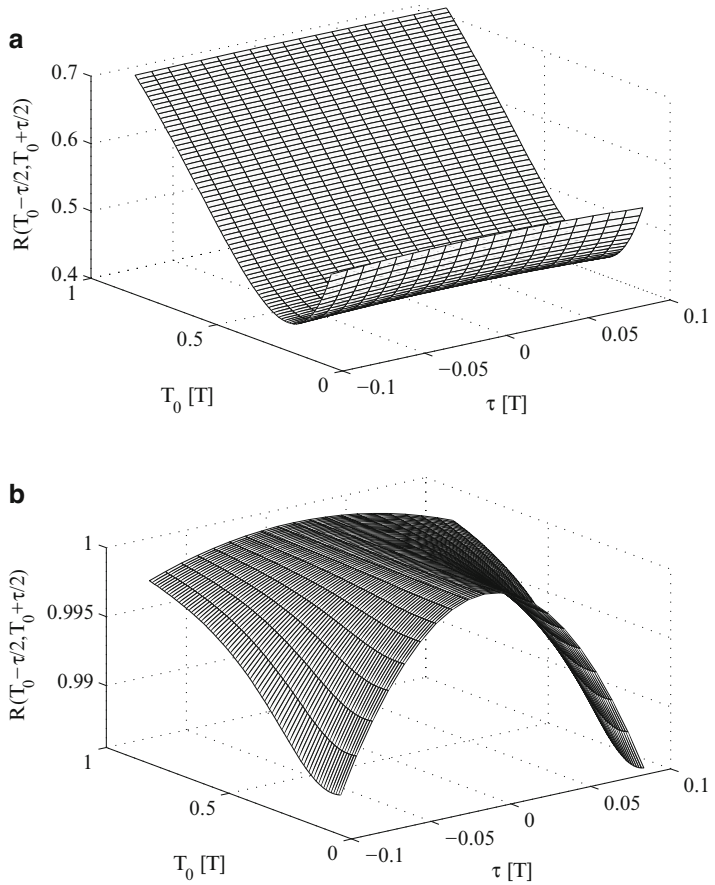

Fig. 2.16 Autocorrelation function $R(T_0 + \tau/2, T_0 - \tau/2)$ as a function of the sampling point T_0 and skew τ. Input signal is WSCS and has an autocorrelation function as in (A.11), with $\omega_{3\text{dB}} = 2/T$. (**a**) The actual autocorrelation function. (**b**) The autocorrelation function normalized such that $R(T_0, T_0) = 1$

$$\begin{aligned} x(t) &= s(t) * h(t) \\ &= \sum_{m=-\infty}^{\lfloor t/T \rfloor} c_m p(t - mT) * h(t) \\ &= \sum_{m=-\infty}^{\lfloor t/T \rfloor} c_m f(t - mT) \end{aligned} \tag{2.83}$$

where $f(t)$ is the pulse response, defined by $f(t) = p(t) * h(t)$.

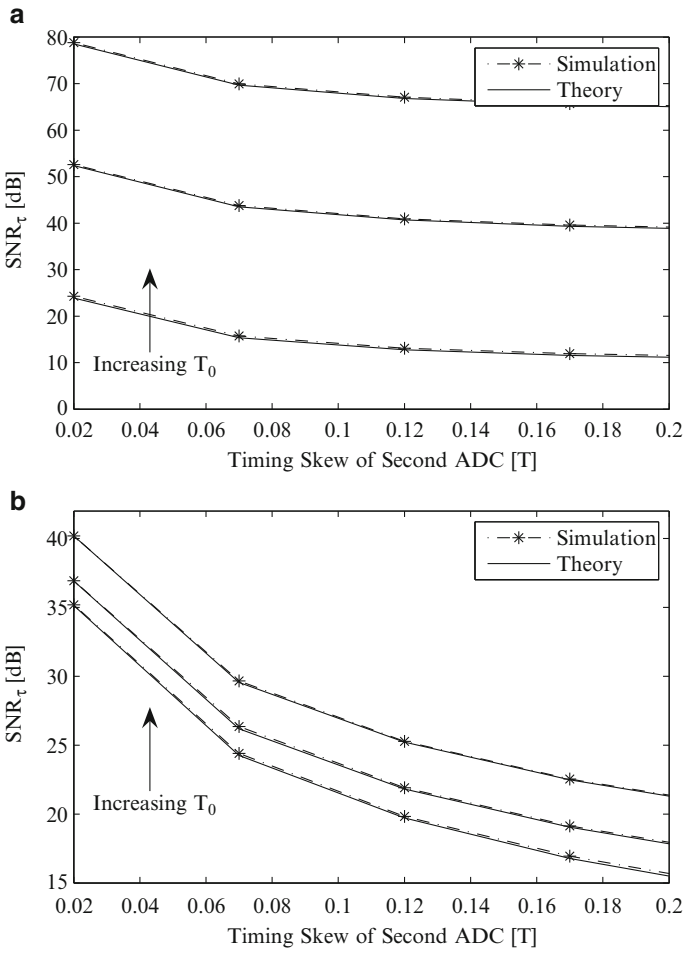

Fig. 2.17 Comparison of theoretical and simulation based SNR_τ. Input signal is WSCS and has an autocorrelation function as in (A.11). (**a**) With $\omega_{3\text{dB}} = 10/T$. (**b**) With $\omega_{3\text{dB}} = 1/T$

In this example, the channel $h(t)$ is a first-order low pass filter such that $h(t) = e^{-(t\omega_{3\text{dB}})}u(t)$. The autocorrelation function of $x(t)$ is

$$R(t_1, t_2) = E[x(t_1)x(t_2)] \tag{2.84}$$

and is fully derived in Appendix A, where it is also shown that $x(t)$ is WSCS.

An example of $R(t_1, t_2)$, where $t_1 = T_0 - \tau/2$ and $t_2 = T_0 + \tau/2$, is shown in Fig. 2.16a as a function of T_0 and the skew τ for $\omega_{3\text{dB}} = 2/T$. Figure 2.16b uses a normalized version of $R(t_1, t_2)$ such that $R(T_0, T_0) = 1$, which illustrates the change in the curvature of the autocorrelation function as a function of T_0.

Without loss of generality, we set τ_0, the timing skew of the first sub-ADC, to 0. Varying the timing skew of the second sub-ADC τ_1 allows us to compare the theoretical results using (A.11) and simulation based results for different values of $\omega_{3\text{dB}}$ and T_0, the ideal sampling point of the sub-ADCs, as in Fig. 2.17. In this simulation, T_0 is varied from $0.1T$ to $0.7T$.

As is expected, the value of T_0 affects the value of the resulting SNR_τ because of its effect on the shape of the autocorrelation curve. This effect depends on the "speed" of the channel; for example, when the channel is extremely fast, as in Fig. 2.17a (where $\omega_{3\text{dB}} = 10/T$), the effect is much larger than with an extremely slow channel, as in Fig. 2.17b (where $\omega_{3\text{dB}} = 1/T$). Because of the channel used in this example, increasing T_0 from 0 to T results in an increasing SNR_τ; however, this cannot be generalized to all channels.

2.4 Summary

In this chapter, a model for time-interleaved ADCs was presented. Frequency domain analysis was used to illustrate how time-varying errors, such as gain, offset, and timing skew, affect the resulting time-interleaved ADC output. Expressions relating the different errors to ADC performance and bounds on the magnitude of these errors were also derived, and simulations were used to demonstrate the accuracy of these expressions. Thus, for the given set of ADC specifications required by serial links, these expressions are used to calculate the acceptable timing skew, such that it does not limit the performance of the time-interleaved ADC.

http://www.springer.com/978-1-4614-1510-7

Background Calibration of Time-Interleaved Data Converters

El-Chammas, M.; Murmann, B.

2012, XX, 124 p., Hardcover
ISBN: 978-1-4614-1510-7